Autogenous deformation induced- stress evolution in high-volume GGBFS concrete Macro-scale behavior and micro-scale origin

Liang, Minfei; Chang, Ze; Zhang, Yu; Cheng, Hao; He, Shan; Schlangen, Erik; Šavija, Branko

DOI
10.1016/j.conbuildmat.2023.130663

Publication date
2023

Document Version
Final published version

Published in
Construction and Building Materials

Construction and Building Materials 370 (2023) 130663

Contents lists available at ScienceDirect

Construction and Building Materials

journal homepage: www.elsevier.com/locate/conbuildmat

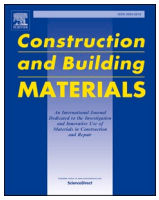

Autogenous deformation induced- stress evolution in high-volume GGBFS concrete: Macro-scale behavior and micro-scale origin

Minfei Liang, Ze Chang *, Yu Zhang, Hao Cheng, Shan He, Erik Schlangen, Branko Šavija

Faculty of Civil Engineering and Geosciences, Delft University of Technology, Delft 2628, CN, the Netherlands

ARTICLE INFO

Keywords:
GGBFS concrete
Early-age cracking
Autogenous deformation
Stress evolution

ABSTRACT

This study aims to experimentally investigate the autogenous deformation and the stress evolution in restrained high-volume ground granulated blast furnace slag (GGBFS) concrete. The Temperature Stress Testing Machine (TSTM) and Autogenous Deformation Testing Machine (ADTM) were used to study the macro-scale autogenous deformation and stress evolution of high-volume GGBFS concrete with w/b ratios of 0.35, 0.42, and 0.50. The early-age cracking (EAC) risk (quantified by stress-strength ratio) and stress relaxation were analyzed extensively based on ADTM and TSTM results. Furthermore, Environmental Scanning Electron Microscopy (ESEM), X-ray Diffraction (XRD), and Mercury Intrusion Porosimetry (MIP) were conducted to explore the micro-scale origin of the autogenous deformation of high-volume GGBFS concrete, which supports the observations on the macroscale measurement of TSTM/ ADTM tests. This study finds that the ettringite formation in the first two days results in autogenous expansion, which can delay the appearance of tensile stress. The magnitude of autogenous expansion depends on the compatibility of ettringite content and pore size. The w/b ratio of 0.42 turns out to be optimal because it produces the highest amount of ettringite and results in the highest autogenous expansion. In comparison, the w/b ratio of 0.35 introduces significant autogenous shrinkage after the expansion peak and therefore corresponds to a high early-age cracking risk.

1. Introduction

With regard to the worldwide concern of carbon reduction, ground granulated blast furnace slag (GGBFS) has been proven to be an effective alternative cementitious material to ordinary Portland cement (OPC). In total, the manufacturing process of OPC accounts for 5–8 % of worldwide yearly carbon dioxide emissions, and therefore reducing the use of OPC is a main target in the campaign for carbon reduction. Normally, GGBFS can replace 35–70 % OPC in concrete. Compared to OPC concrete, the addition of GGBFS improves the fresh workability [1] and shows comparable or even higher compressive strength [2], flexural strength [3] and elastic modulus [4] at later ages.

Early-age cracking (EAC) is a significant engineering problem in the construction of concrete structures. The continuous hydration of hardening cementitious materials results in heat release and self-desiccation, which causes volumetric deformation of concrete structures. If the volumetric deformation is restrained, stresses occur and may harm the integrity of concrete structures. Since the addition of GGBFS significantly alters the cementitious system, its influence on the resistance of concrete structures to EAC is also essential. Such influence can be summarized mainly in two aspects: volumetric deformation and mechanical properties, which together determine the evolution of early-age stress (EAS). Studies [5–7] have confirmed that the addition of GGBFS effectively reduces the hydration heat and thereafter reduces the thermal shrinkage. However, due to the pozzolanic reaction and finer pore structure, the effect of self-desiccation is enhanced by GGBFS, causing a faster drop of internal relative humidity [8–10]. As a result, the addition of GGBFS increases autogenous shrinkage, which happens almost uniformly and can cause through cracks [11]. Therefore, increasing the content of GGBFS brings risks of autogenous shrinkage-induced EAC. In this regard, the EAS evolution of high-volume GGBFS concrete, which directly links to the EAC risk, deserves thorough and in-depth research.

Experiments have been carried out to investigate the influence of GGBFS on EAC risk. Based on Temperature Stress Testing Machine (TSTM), Shen et al. [12] conducted a uniaxial restrained test on High-Performance Concrete (HPC) with GGBFS ranging from 0 % to 50 %. Their experimental results confirmed the benefits of GGBFS in reducing early-age thermal shrinkage. Moreover, it was shown that the EAC risks

* Corresponding author.
E-mail addresses: M.Liang-1@tudelft.nl (M. Liang), z.chang-1@tudelft.nl (Z. Chang), Y.Zhang-28@tudelft.nl (Y. Zhang), H.Cheng-2@tudelft.nl (H. Cheng), S.He-2@tudelft.nl (S. He), Erik.Schlangen@tudelft.nl (E. Schlangen), B.Savija@tudelft.nl (B. Šavija).

https://doi.org/10.1016/j.conbuildmat.2023.130663
Received 22 November 2022; Received in revised form 5 February 2023; Accepted 6 February 2023
Available online 11 February 2023

increase with the increasing GGBFS content, and the optimal content of GGBFS was found to be 20 %. By measuring the free and restrained shrinkage of paste with a w/c ratio of 0.32, Bouasker et al [13] found that, although finer pore structure induces higher autogenous shrinkage, the GGBFS cement paste often exhibited later EAC than OPC paste. Similarly, Darqueennes et al [14] conducted a TSTM test on GGBFS concrete with w/c ratio of 0.43 and concluded that GGBFS concrete cracks later than OPC concrete. This was explained by the early-age expansion and high creep/ relaxation of the GGBFS cement matrix. Shen et al. [15] conducted restrained ring tests on GGBFS concrete with GGBFS content varying from 0 to 50 % and also found that the increasing content of GGBFS decreased the EAC risk. Under semi-adiabatic conditions, Wei et al. [16] carried out uniaxial restrained tests and concluded that, although the thermal shrinkage can be effectively reduced, the major reasons accounting for EAC of GGBFS concrete lay in the consistent autogenous shrinkage. Focusing on the influence of slag composition, Markandeya et al [17] conducted TSTM tests on GGBFS concrete using GGBFS with different MgO/Al_2O_3 ratios, but with similar Ca/SiO_2 ratios. Their results showed that a low MgO/Al_2O_3 ratio can result in high autogenous shrinkage and therefore promote the EAC risk. Overall, existing studies report contradictory conclusions on whether the addition of GGBFS increases the EAC risk or not, compared with the OPC concrete. Such disagreement is understandable considering the difference in testing details, including the thermal boundaries, material differences, etc. For example, in non-isothermal conditions, the addition of GGBFS surely decreases EAC risk since thermal shrinkage is highly reduced. Such declaration is mostly tenable in massive concrete structures where thermal shrinkage dominates. However, for medium- or thin-concrete structures, autogenous shrinkage, which is inevitable and can induce stress consistently, can play a more important role in EAC risk.

Despite the disagreement, one consensus existing in the aforementioned studies on restrained tests is the increasing autogenous shrinkage induced by GGBFS. Many studies solely about autogenous shrinkage have also validated this conclusion [8–10,18–20]. Recently, Hilloulin et al. [21] trained Machine Learning models on 1889 shrinkage data and conducted a thorough dependence analysis on the influence of various ingredients on shrinkage. Based on a comprehensive database and advanced Machine Learning algorithms, their results proved that increasing GGBFS content can lead to higher shrinkage. To leverage the environmental benefits, the EAC risks of high-volume GGBFS concrete induced by autogenous shrinkage need to be addressed. However, existing studies about EAC mostly concentrated on GGBFS concrete with a medium percentage of OPC replacement (0 ~ 50 %). Meanwhile, strict thermal boundary conditions were often unreachable, making it difficult to fully decouple the influence of autogenous and thermal shrinkage. Most importantly, the EAC analysis of GGBFS concrete with different w/b ratios, which is important for the practical application of high-volume GGBFS concrete, is scarce.

Accordingly, TSTM tests are performed herein to figure out the autogenous shrinkage and EAS evolution of high-volume GGBFS concrete with a 70 % replacement rate of OPC and w/b ratio ranging from 0.35 to 0.5. In addition, an OPC concrete mix is tested as a reference. A thorough analysis of the coupling influence of autogenous shrinkage, elastic modulus, and stress relaxation on EAS evolution was conducted. MIP, XRD, and ESEM tests were performed to provide an in-depth understanding of the autogenous deformation of high-volume GGBFS concrete with different w/c ratios. The aforementioned testing results aim to provide an in-depth understanding of autogenous shrinkage-induced EAC risk of high-volume GGBFS concrete with different w/b ratios.

2. Experimental

2.1. Materials

Using the CEM III/B 42.5 as the cementitious material, which contains 30 % OPC and 70 % GGBFS, three mixes with the w/b ratios of 0.35, 0.42, and 0.50 were studied. Meanwhile, a reference mix using CEM I 42.5 as the cementitious material and a w/b ratio of 0.42 was also incorporated. Both CEM III/B and CEM I used in this paper were supplied by the Eerste Nederlandse Cement Industrie (ENCI). The detailed mixture proportions are shown in Table. 1, and are properly labeled to show the difference in cementitious materials and w/b ratio. For example, “C3-50” stands for the mix using CEM III/B with a w/b ratio of 0.50. The main chemical compositions of utilized CEM III/B 42.5 and CEM I 42.5 are listed in Table. 2. Superplasticizer (SP) MasterGlenium 51 with a water-reducing rate of 35 % was used for mixes with w/b = 0.42 and 0.35. The compressive strength of each mix was tested on three cubic samples with a side length of 150 mm at ages 1, 3, 7, 14, and 28 days. The testing results of compressive strength are shown in Fig. 1. To keep comparable compressive strength, the clinker in CEM III/B 42.5 is finer than that of CEM I 42.5. Therefore, for w/b = 0.42, the compressive strength of CEM III/B 42.5 mixes are lower than that of CEM I 42.5 on the first day, but notably higher after 3 days [14,22].

2.2. ADTM and TSTM tests

To test the autogenous deformation and the stress it induces, the Autogenous Deformation Testing Machine (ADTM) and Temperature Stress Testing Machine (TSTM) were developed [23]. In this study, we conducted the ADTM and TSTM tests for the aforementioned mixes by following the workflow in Fig. 2. Two wooden molds with low heat conductivity were used for casting of prism and dog-bone specimens, which were then sealed and tested under free and restrained conditions respectively. Isothermal conditions were ensured by circulating temperature-regulated water around the concrete specimens in wooden molds.

The ADTM for testing the autogenous deformation of concrete is shown in Fig. 3. Wood plates with low conductivity were assembled to form a mold for casting prismatic samples with the size 1000 *150 *100 mm^3. By wrapping the sample with plastic films, moisture exchange with the environment was prevented so that the drying shrinkage was excluded. To exclude the influence of temperature, temperature-regulated water was circulated in the surrounding wood mold through the embedded water channel (Fig. 3(c)) to keep the temperature of the specimen at a constant value. A steel plate was applied on the inner surface of the wood mold to enable fast heat conduction (Fig. 3(d)). Three thermo-couples were embedded in the prismatic sample to monitor the temperature development, as shown by the red dots in Fig. 3 (a). A feedback loop between the measurement of the middle thermo-couple and an externally-connected cryostat was built to regulate the water temperature and stabilize the temperature of the sample at 20 degrees. Four Linear Variable Differential Transformers (LVDTs) were configured at two sides of the sample and the average of the deformation

Table 1
Mixes for TSTM tests (kg/m^3).

Sample	Cement type	Cement	w/b	Sand (0–4 mm)	Gravel (4–16 mm)	SP	Slump (mm)
C3-50	CEM III/B	320	0.50	811.8	1032	0	90
C3-42	CEM III/B	320	0.42	811.8	1032	0.475	60
C3-35	CEM III/B	320	0.35	811.8	1032	1.900	40
C1-42	CEM I	320	0.42	811.8	1032	0.475	50

Table 2
Main compositions of utilized cementitious materials (wt.%).

Composition	CEM III/B	CEM I
CaO	47.11	64.00
SiO_2	29.11	20.00
Al_2O_3	10.02	5.00
MgO	5.89	–
SO_3	2.82	2.93
Fe_2O_3	1.19	3.00
Na_2O	0.28	0.58

at the two sides was taken as the measurement of autogenous shrinkage. The LVDTs on the same side were connected with a quartz bar, which has a low coefficient of thermal expansion so that any potential change of mounting base due to heat change cannot influence the deformation measurement. With the measures above, the influence of thermal and drying deformation can be excluded, and the autogenous deformation can be measured.

The TSTM (Fig. 4) is used to restrain autogenous deformation and measure stress development. In TSTM, the principles of the mold assembly, water circulation, and LVDT configurations are the same as the ADTM introduced above. The load applied by the actuator was continuously adjusted to keep the deformation of the specimens measured by four LVDTs at 0, based on a Proportion Integration Differentiation (PID) control algorithm. To ensure that all autogenous deformation-induced stress is accounted for, the TSTM test has to be started before the concrete hardens [24]. In this study, the TSTM tests were started 7.0 h after casting, which is earlier than the final setting time of the cement paste of all studied mixes. Before the timing when LVDTs can be set up, the load was controlled by the displacement of the clamping head measured by 2 LVDTs. Afterward, the 4 LVDTs at the two sides of TSTM were set up and used to control the load. During the first stage, when the concrete was far from hardened (within the first 7 h after casting), the stress measured was less than 0.01 MPa, and therefore only the stress after 7 h was accounted for in the experimental results of this paper. Due to uncontrollable factors such as power-off, the testing duration for each test differs, ranging from 647 h to 804 h.

2.3. Corrugated tube test

In the process of autogenous deformation, the aggregate mainly plays the role of restraint [25], while the autogenous deformation mainly originates from the cement paste. Therefore, it is also important to measure the autogenous deformation of cement paste. Considering this paper is mainly about the influence of GGBFS, only relevant mixes were incorporated into this test. Hence, the corrugated tube tests [26] were conducted to measure the autogenous shrinkage of cement paste of C3-35, C3-42, and C3-50 immediately after casting time.

2.4. Material characterization

Material characterization tests aim to find microscale origins that explain the corresponding macroscale behavior (i.e., autogenous deformation and EAS) of high-volume GGBFS concrete. By analyzing the consumption of C_3A and C_4AF, Darquennes et al [14] inferred that the autogenous expansion in GGBFS concrete is a result of ettringite formation. Indeed, as the most active phase of clinker, the C_3A begins immediately to react with gypsum and forms ettringite once it dissolves in water. According to [27], the additional sulfur and alumina in GGBFS can highly promote ettringite formation. Afterward, ettringite tends to grow in the pores and expand, applying crystalline pressure on the pore wall, which then induces autogenous expansion. Hence, the magnitude of autogenous expansion depends on the volume/ amount of ettringite and the pore size distribution [28]. In other words, autogenous

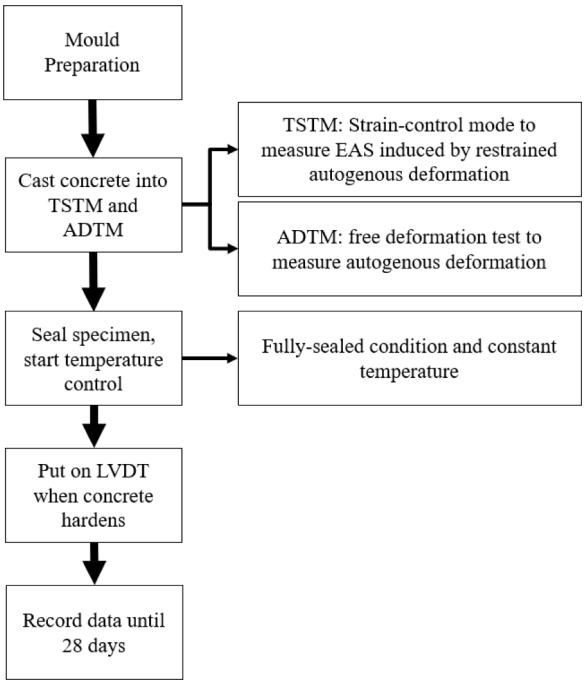

Fig. 2. ADTM and TSTM testing procedure.

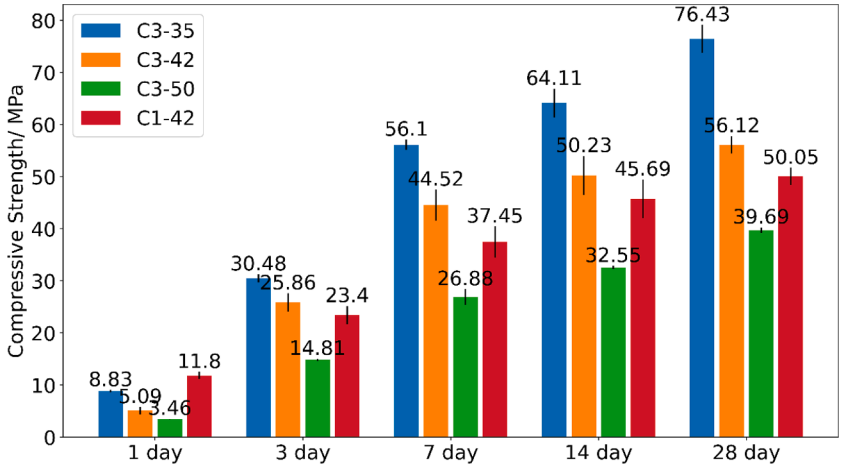

Fig. 1. Compressive strength.

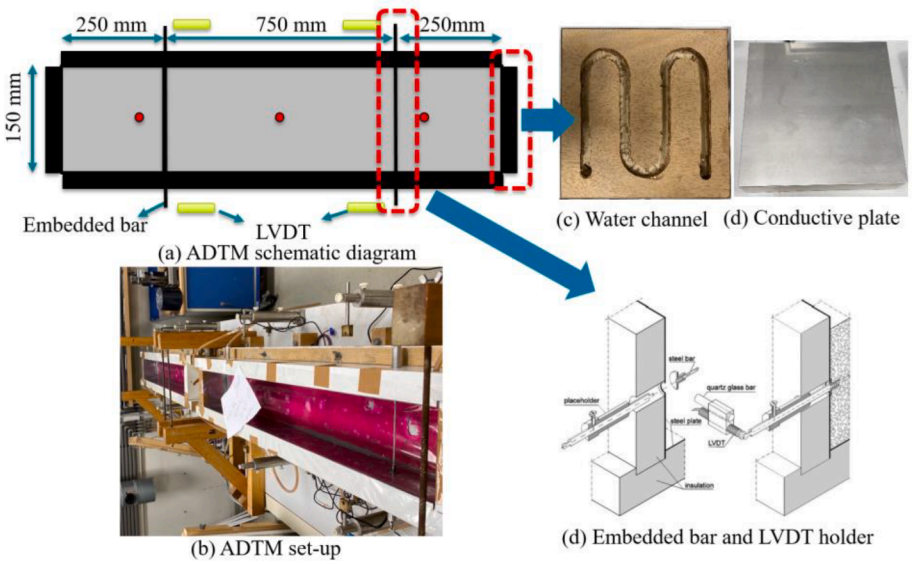

Fig. 3. Autogenous Deformation Testing Machine (ADTM).

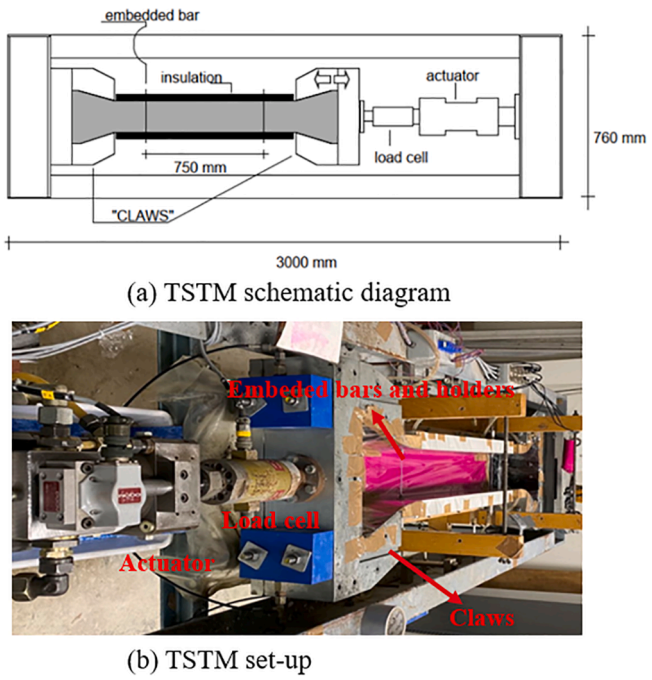

Fig. 4. Temperature Stress Testing Machine (TSTM).

expansion can happen only when the volume of ettringite is sufficient to fill the pores. To investigate the effects of ettringite formation on autogenous expansion more straightforwardly and comprehensively, we employed ESEM to qualitatively study the distribution of ettringite and QXRD/ MIP to quantitatively analyze the change of ettringite amount and pore structure. In this section, the cement paste of the three mixes containing GGBFS C3-35, C3-42, and C3-50 was tested. Each sample was cast and cured at a room temperature of 20 degrees and the hydration kinetics was stopped at the desired ages using the solvent exchange with isopropanol.

Since the autogenous deformation is driven by the capillary tension induced by self-desiccation and can be well explained by Kelvin's Law [29–31], the pore structure evolution is important for the analysis of the autogenous deformation process. Accordingly, the mercury intrusion porosimetry (MIP) test was conducted. Specimens were crushed into small pieces and stored in the vacuum container to get rid of isopropanol after the hydration was stopped. Note that in the MIP test, it is necessary to use small pieces of specimens (with a size typically smaller than 4 mm) to avoid the influence of ink-bottle pores [32]. According to [32], it is optimal to prepare the sample with a low-rate cutting process. However, in our study, the specimens younger than 3 days were too soft to bear the clamping force applied by the cutting machine, as well as the cutting force. Instead, the specimens were soft enough to be easily crushed into small pieces with a gentle force by a steel block. Note that due to the damage induced in the sample preparation process and the assumption and limitations of the MIP test itself [33,34], the results herein do not necessarily represent the absolute value of the true pore size distribution. However, considering that all specimens undergo the same process, qualitative results regarding the pore structures will still be comparable, allowing for further analysis of the influence of pore structures on autogenous deformation. The intrusion process of the mercury was described in the following three steps: 1) a low-press state from 0 to 0.170 MPa; 2) a high-pressure state from 0.170 to 210 MPa; 3) an unpressurized state from 210 to 0.170 MPa. The pore radius was calculated based on the Washburn equation, with the surface tension of mercury being 0.485 N/m and the contact angle between mercury and sample being 140° [35].

Besides, as the hydration products also directly influence the autogenous deformation process, scanning environmental microscopy (SEM) and X-ray diffraction (XRD) were conducted to analyze the evolution of microstructure and chemical compositions. For SEM, 2 mm-thick samples were grinded using 4000 grit abrasive paper for 5 min and polished using synthetic silk polishing cloth (MD-Dac from Struers) charged with 3 μm and 1 μm diamond pastes for 2 separate 30-minute sessions. During the grinding and polishing processes, an oil-based lubricant (DP-Lubricant Brown from Struers) was used to dissipate the heat build-up. Between each grinding and polishing interval, the sample was immersed in an ultrasonic bath filled with pure ethanol for 30 *sec* to remove debris. Afterward, samples were carbon coated and moved into an FEI QUANTA FEG 650 ESEM. An accelerating voltage of 10 kV and a working distance of 10 mm were used throughout the research. For XRD test, it was carried out on a Philips PW 1830/40 powder diffractometer using the Cu K-alpha radiation. The adopted acceleration voltage was 40 kV and the X-ray beam current was 40 mA. The XRD data were collected with a step size of 0.03° for a 2θ range from 5° to 80°.

3. Results

3.1. Autogenous deformation

The autogenous deformations measured by the ADTM are shown in Fig. 5. The results show that the autogenous deformation of all 4 mixes is characterized by an autogenous expansion phase in the first 1 ~ 3 days, and then autogenous shrinkage starts. For the mix C3-50, a second expansion peak can be observed, which resembles the second peak of the heat release rate of GGBFS concrete [36,37] and therefore may be attributed to the continuous hydration of slag after the first day. For the mixes C3-35, C3-42, C3-50, and C1-42, the expansion peak of 52.4, 84.8, 55.3, and 28.9 μ-strain are reached at 40, 38, 27, and 33 h, respectively. Comparing the expansion phase of the 4 mixes, the following patterns can be observed:

i. Significant autogenous expansion in the first two days characterized the autogenous deformation process. The magnitudes of early autogenous expansion for C1-42, C3-42, and C3-50 are higher than the later autogenous shrinkage. For C3-35, the autogenous expansion is compensated by a fast shrinkage process at a later age (around 600 h).
ii. The high-volume GGBFS mixes show much higher expansion than the OPC mix.
iii. For the GGBFS mixes, C3-42 shows higher expansion than the others. C3-50 and C3-35 have a similar expansion magnitude, but C3-50 shows a longer expansion phase.

Taking the first expansion peak as time-zero, the shrinkage process of the 4 mixes is shown in Fig. 6. The results show that, after the expansion peak, all high-volume GGBFS mixes show higher autogenous shrinkage than the OPC mix, which is in accordance with existing studies [38,39]. Within the first 100 h, the high-volume GGBFS concrete with a low w/b ratio (C3-35) shows drastic autogenous shrinkage, and afterward similar shrinking rate can be observed for the 3 GGBFS concrete. With a higher w/b ratio, C3-50 gains a second expansion peak, which seems to be favorable for avoiding EAC. A slightly faster shrinking rate is also observed for C3-50 when compared with the mix of a lower w/b ratio C3-42. This contradicts existing studies [40,41] which concluded that a lower w/b ratio corresponds to lower porosity and smaller pore size, and should have higher autogenous shrinkage. However, due to the limitations (e.g., temperature instability and friction) of ADTM, the autogenous deformation curve is not smooth, and considering the measurement error that may be involved, the slight difference between the shrinking phase of C3-42 and C3-50 should not be seen as significant.

The autogenous deformation of the cement paste of C3-35, C3-42, and C3-50 is measured by corrugated tube test [26], as shown in Fig. 7. Note that due to the incorporation of the aggregate and much smaller sectional size of specimens used in the corrugates tube test, the absolute values of the autogenous deformation measured by ADTM are significantly lower than that by corrugate tube tests. Fig. 7(a) shows the autogenous deformation curve by setting the time-zero the same as the ADTM, and Fig. 7(b) shows the autogenous deformation after the expansion peak. The results of all 3 GGBFS cement pastes resemble the behavior of their concrete counterparts: at first, an expansion phase lasts around 30 h, and then the shrinkage phase starts. Similar to the results of concrete, the C3-42 gains the highest expansion peak and the C3-50 shows a lower shrinking rate after the first expansion peak. However, due to the effects of dilution and restraint incorporated by aggregate and the interfacial transition zone, the results of paste still preserve obvious differences with concrete: 1) the expansion peak of C3-50 is notably higher than C3-35, and the second expansion peak seems to be less obvious; 2) the shrinking rate of C3-42 is higher than C3-50.

Overall, the results show that autogenous deformation of high-volume GGBFS mix is characterized by a high expansion peak, which can delay the appearance of tensile stress at an early age and therefore reduce the EAC risk. After the expansion peak, the GGBFS mixes undergo a faster autogenous shrinkage than the OPC mix. Especially for concrete with a low w/b ratio at 50 ~ 150 h, the drastic autogenous shrinkage indicates a high EAC risk. Comparing all the GGBFS mixes, both paste and concrete results indicate that the mix with a medium w/b ratio (i.e., 0.42) shows the highest expansion that can ease the EAC risk.

3.2. Stress evolution

3.2.1. Stress results

Under isothermal conditions ensured by water circulation, wood mold insulation, and constant room temperature, the autogenous deformation is restrained by the TSTM and the induced stress is shown in Fig. 8. The stress evolution resembles the pattern observed in autogenous deformation results: all mixes display an initial compression phase and then go to tension phase. The expanding and shrinking process observed in ADTM corresponds well with the stress decrease (i.e., compression) and increase (i.e., tension) observed in TSTM respectively. The initial compression phase has a similar duration with the autogenous expansion measured by the ADTM, which proves the validity of combining ADTM and TSTM testing. Comparing the TSTM results, the following pattern can be observed:

i. The GGBFS mix with a low w/b ratio C3-35 shows a fast increase of stress among 50–150 h, which indicates a high risk of EAC.
ii. The OPC mix C1-42 shows the shortest expansion phase and slowest stress evolution rate, which is even slower than the GGBFS mix with a higher w/b ratio (C3-50).
iii. The GGBFS mix with medium w/b ratio C3-42 obtains compressive stress that is similar to C3-35. Note that although C3-42 has

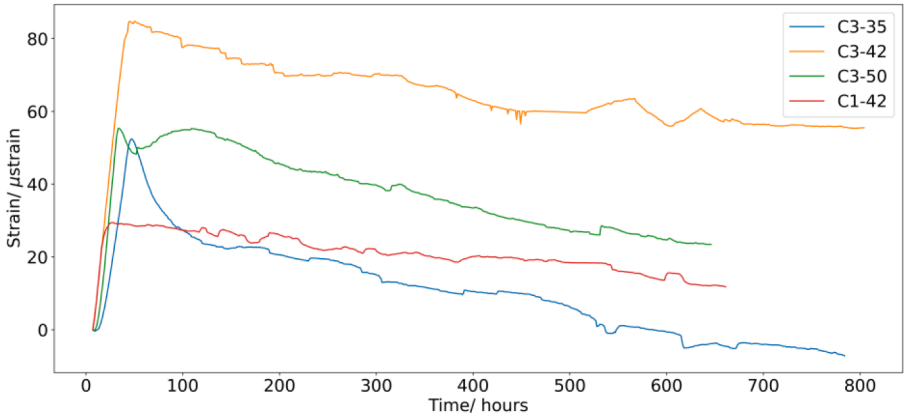

Fig. 5. Autogenous deformation measured by ADTM.

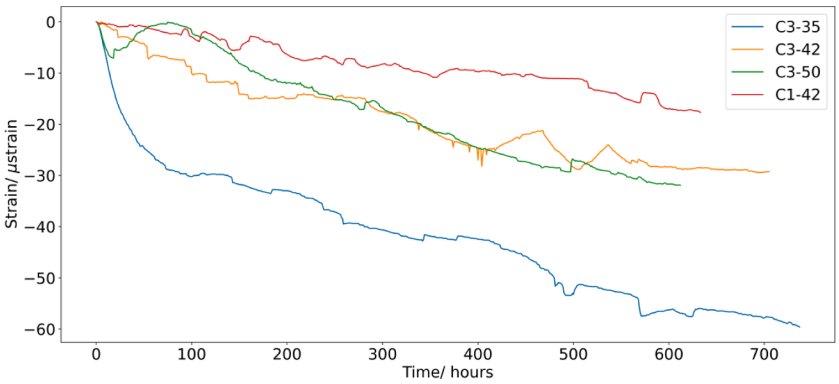

Fig. 6. Autogenous shrinkage zeroed at the expansion peak.

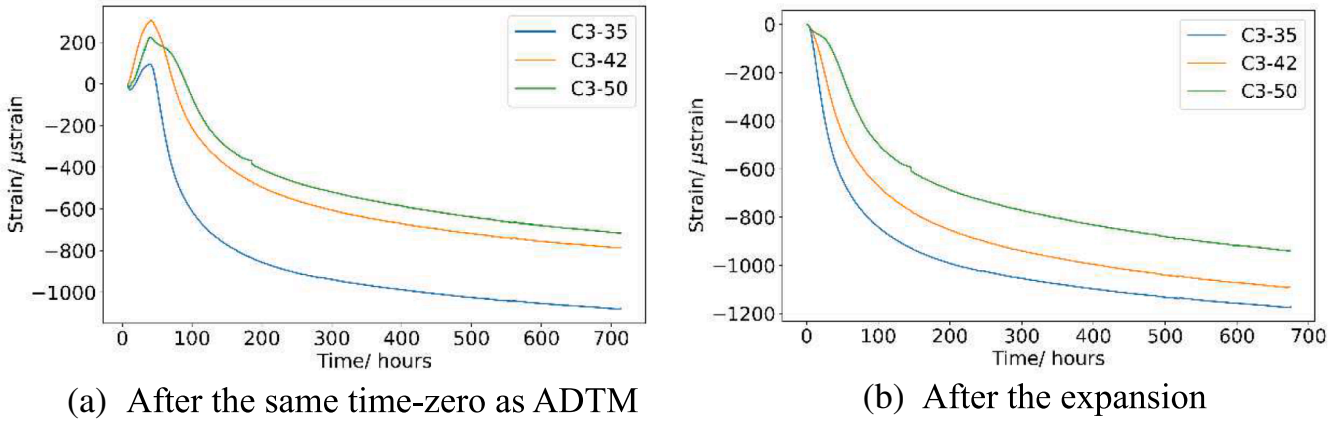

Fig. 7. Autogenous shrinkage zeroed at the expansion peak.

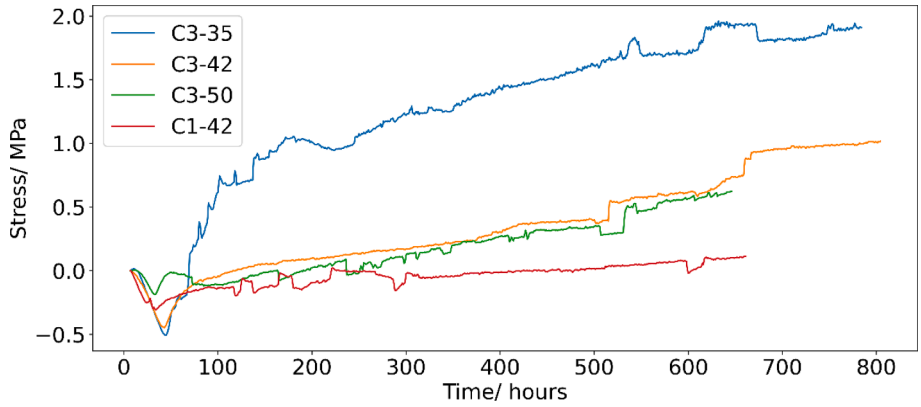

Fig. 8. Stress evolution in restrained concrete measured by TSTM.

much higher expansion as measured in ADTM, the lower elastic modulus and higher relaxation (see later in section 3.2.3) limits the compressive stress level that can be induced by the restrained expansion. However, compared to C3-50, the compressive stress in C3-42 is noticeably higher, which compensates for more shrinkage-induced tensile stress after the expansion peak and finally leads to a similar tensile stress level.

3.2.2. *Stress-strength ratio*

To more accurately compare the EAC risk at different ages, the stress-strength ratio is a straightforward index. The tensile strength of concrete is closely correlated with the compressive strength and can be predicted accurately by a closed-form formula [42–44]. To evaluate the EAC risk quantitatively, this paper implements the formula proposed by the Model Code 2010 [45] to estimate the development of splitting tensile strength as follows:

$$f_{ct}(t) = \begin{cases} 0.3 \times f_c^{\frac{2}{3}}, f_c < 50MPa \\ 2.12 \times ln(1 + 0.1 \times f_c)\ f_c \geq 50MPa \end{cases} \quad (1)$$

where $f_{ct}(t)$ is the estimated tensile strength at the age of t hours; f_c is the compressive strength measured at t hours, as shown in section 2.1. In this study, the compressive strength tested at 1, 3, 7, 14, and 28 days is used to estimate the tensile strength at corresponding ages, and then a quadratic spline [46] is conducted to interpolate the estimated tensile strength in a continuous time range. By dividing the stress results of

Fig. 8 with the estimated tensile strength, the stress-strength ratio of the 4 mixes is shown in Fig. 9. Note that the negative values in Fig. 9 mean that the sample is in a compressive phase and therefore represent no EAC risk. The stress-strength ratio of the mix C3-35, C3-42, C3-50, and C1-42 exceeds 0 at 70, 127, 200, and 412 h, respectively, which denotes the timing when tensile stress starts to accumulate. The stress-strength ratio results show a similar but more straightforward and clearer pattern than the stress results as follows:

i. The stress-strength ratio of the mix C3-35 shows a fast-increasing rate before 150 h and a steady increasing stage afterward. A value of 0.417 is reached at 785 h. In practical engineering design normally the limit state value of the tensile stress-strength ratio is given as 0.5. Moreover, the value 0.417 only represents the percentage of autogenous shrinkage-induced stress in tensile strength under a favorable curing temperature of 20 degrees, while the stress that may be induced by thermal and drying shrinkage and designed loads are not accounted for. Therefore, the stress-strength value of the mix C3-35 indicates a high EAC risk.
ii. The OPC mix shows tensile stress at the latest age and reaches a stress-strength ratio of 0.018 at 691 h, which proves that autogenous shrinkage-induced stress has negligible influence on the EAC of OPC concrete with a medium w/b ratio (0.42).
iii. Although the tensile stress in C3-42 appears earlier than C3-50, their stress-strength ratio maintains at a level lower than 0.2 at the first 672 h and shows a similar increasing rate.

3.2.3. Relaxation

Stress relaxation is a significant factor that must be considered in the quantification of early-age stress evolution in restrained concrete since the creep/ relaxation of early-age concrete is very high [47–49]. Due to the difficulties of continuous measurement of aging creep/ relaxation, the inverse modeling by Bayesian Optimization can be applied in TSTM tests, referring to the author's previous study [50]. Besides, minute-long creep tests [51,52] can also be applied since setting time. In this paper, we aim to provide a qualitative understanding of how relaxation influences stress accumulation. Because the stress level is under 50 % of tensile strength, it is reasonable to assume an ideal viscoelastic constitutive model of concrete. Thereby, the stress is formed by the elastic part σ_{el} and relaxed part σ_{re}, expressed as:

$$\sigma(t) = \sigma_{el}(t) - \sigma_{re}(t) \tag{2}$$

where σ(t) is the overall stress measured by the TSTM tests. If the aging relaxation modulus or the aging creep compliance is known, following the Boltzmann superposition, the total stress can also be expressed as the following convolution:

$$\sigma(t) = \int_0^t R(t,t')\dot{\varepsilon}(t')dt' \tag{3}$$

where $R(t,t')$ represents the aging relaxation modulus at time t when the load is applied at t'; ε represents the enforced strain. To account for the influence of relaxed stress on the overall stress evolution, we directly calculate the relaxed stress by subtracting the elastic stress from the overall stress measured by the TSTM. The elastic stress can be calculated as:

$$\sigma_{el}(t) = \int_0^t E(t)\dot{\varepsilon}(t)dt \tag{4}$$

where E is the elastic modulus. Applying the mid-point rule and assuming the time step Δt as 1 h, the calculation of Eq(4) can be expressed as:

$$\sigma_{el}(t) = \sum_0^t E(t+\frac{1}{2}\Delta t) \times \Delta\varepsilon(t) \times \Delta t \tag{5}$$

Substituting Eq(5) in Eq(2), the relaxed stress can be expressed as:

$$\sigma_{re}(t) = \sum_0^t E(t+\frac{1}{2}\Delta t) \times \Delta\varepsilon(t) \times \Delta t - \sigma(t) \tag{6}$$

Due to the close correlation with compressive strength [53–55], the elastic modulus $E(t)$ is estimated by applying the formula recommended by the Model Code 2010 [45]. Note that the validity of this estimation was confirmed by comparing the influence of various formulas and the estimated results of the C3-42 with the elastic modulus tests in the authors' previous study [50]. The formula used for estimating the elastic modulus is as follows:

$$E(t) = E_{c0}\alpha_E(\frac{f_c(t)}{10})^{\frac{1}{3}} \tag{7}$$

where E_{c0} is a coefficient and equals 21500 MPa; α_E is the coefficient for different aggregates ranging from 0.7 to 1.2. Considering the aggregates used in the tests are mainly quartzite gravel, α_E equals 1.0 in this study. Following Eq(5 ~ 7), the elastic and relaxed stress can be calculated, as shown in Fig. 10. A significant influence of relaxation on stress accumulation before the expansion peak is observed, which directly results in the decrease of compressive stress and accelerates the occurrence of tensile stress. Afterward, the relaxed stress steadily decreases and most elastic stress is preserved as the total stress. This can also be seen from the similar increase rate of the overall stress and elastic stress. The results here show that the influence of creep/ relaxation on the EAC risk of GGBFS concrete is negative. The high creep/relaxation at an early-age compromise the effect of early-age autogenous expansion reduces the compressive stress in the first 1 ~ 3 days and exposes the restrained concrete to tensile stress earlier. To efficiently and precisely

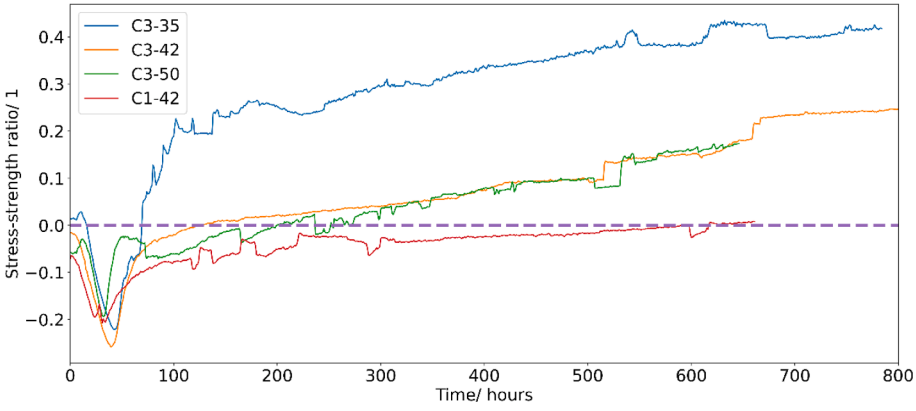

Fig. 9. Stress-strength ratio.

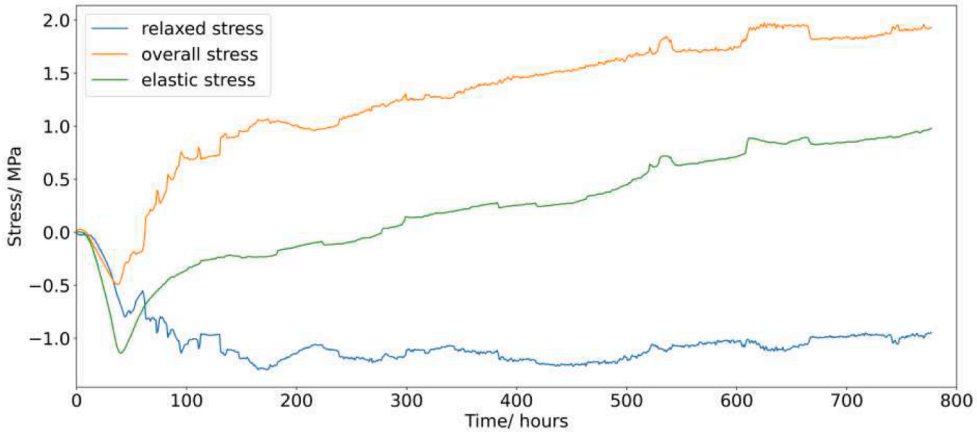

(a) C3-35

Fig. 10. Relaxed stress.

quantify the aging creep/relaxation, one can refer to the authors' previous study [50].

3.3. Autogenous expansion due to ettringite formation

3.3.1. ESEM results

Using ESEM with magnifications of 5000x (left) and 20000x (right), the distribution and morphology of ettringite can be observed. Representative ESEM images of the 3 mixes C3-35, C3-42, and C3-50 at 1 day are shown in Fig. 11. The 5000 × images were taken at porous areas of the samples and the 20000x images were the zoomed-in view of one of the large pores. The 5000x ESEM images show that ettringite mostly appears in porous regions where continuous hydration happens and fibrous CSH grows. The 20000x SEM images show the existence of rod-like ettringite in all mixes. The GGBFS mixes with higher w/b ratios (i.e., 0.42 and 0.50) have more porous areas and tend to obtain more ettringite with larger rod sizes. For the C3-50 mix, scattered ettringite grows in large pores, which indicates limited crystalline pressure and therefore lower autogenous expansion. While for mix C3-42, dense clusters of ettringite with large rod size fill in relatively smaller pores, which indicates considerable crystalline pressure resulting in higher autogenous expansion. These observations are consistent with the aforementioned ADTM and TSTM tests of all 4 mixes. Quantitative evidence will be found in the QXRD and MIP test results as follows.

3.3.2. XRD and Rietveld refinement

The aforementioned ADTM/ TSTM tests show high autogenous expansion in high-volume GGBFS concrete, indicating a high amount of ettringite. Therefore, the GGBFS mixes C3-35, C3-42 and C3-50 were selected to conduct XRD analysis at the age of 2 days. Meanwhile, to distinguish the pattern of how ettringite content evolves with time, the ettringite content of the mix C3-42 at 1, 2, and 3 days were also tested. Before the XRD test, 10 % silicon was added to the sample powder as an internal standard, and then Rietveld refinement [56] was conducted to decompose the raw XRD curve. By predefining the mineral types of different hydration products and clinkers that exist in early-age GGBFS paste, the decomposition is conducted based on the program BGMN [57] and the ICDD database. As shown in Fig. 12, considerably good fitting performance was obtained for all XRD patterns of all samples, whose weighted profile R-factors (R_{wp}) were all lower than 2.0 %.

The intensity of ettringite at 9 degrees measured by the XRD and the mass fraction of ettringite calculated by Rietveld refinement is shown in Fig. 13, which exhibits excellent consistency with the ADTM/ TSTM results in the following 2 aspects:

i. Comparing the GGBFS samples with different w/b ratios at 2 days (i.e., C3-35-2d, C3-42-2d, and C3-50-2d), the sample C3-42-2d contains the highest amount of ettringite. The aforementioned ADTM/ TSTM tests exhibited the consistent pattern that the C3-42 sample obtained the highest expansion peak and high compressive stress.
ii. Comparing the GGBFS samples with the same w/b ratio at 1, 2, and 3 days (i.e., C3-42-1d, C3-42-2d, and C3-42-3d), it is found that a considerable amount of ettringite is produced in the 1st day, and then keep increasing until the 2nd day. Afterward, the amount of ettringite starts to decrease and transform into calcium monosulfoaluminate. This is also consistent with the ADTM/ TSTM finding that the expansion peaks of GGBFS mixes are all on the 2nd day.

3.3.3. MIP results

The pore structure not only influences the capillary tension that can be induced by the self-desiccation but also determines the crystalline pressure that can be generated by the ettringite formation. Given this, the MIP tests are conducted on the 3 high-volume GGBFS cement pastes at 1 and 3 days. The results are shown in Fig. 14∼ Fig. 15. The MIP tests enable the following analysis:

i. The rank of the critical pore entry radius (CPER) (i.e., the point where the steepest slope of the dV/dlogD curve is observed in Fig. 14) is C3-35≪ C3-42 ≤ C3-50. The "≪" means that the CPER of the C3-35 is much smaller than others. The "≤" means that the CPER of the C3-42 is lower than C3-50 after 1 day, but they are close after 3 days. According to Kelvin's Equation, the capillary tension that can be induced by self-desiccation is also dependent on the pore size: smaller pores correspond to higher capillary tension and therefore cause higher autogenous shrinkage. In the ADTM/ TSTS tests, the C3-35 showed the fastest autogenous shrinkage and therefore generated more tensile stress. Overall, based on Kelvin's Equation, the ADTM/ TSTM results of all the GGBFS mixes can be explained by the rank of CPER.
ii. After 1 day, the CPER of the mix C3-42 is lower than that of C3-50, which means that the pore size of C3-42 is generally much smaller than C3-50. Therefore, even though with similar ettringite amounts and overall porosity, the pores of C3-42 are easier to be filled, and more crystalline pressure can be applied to the pore walls. This explains why the expansion peak of the C3-42 is significantly higher than C3-50.

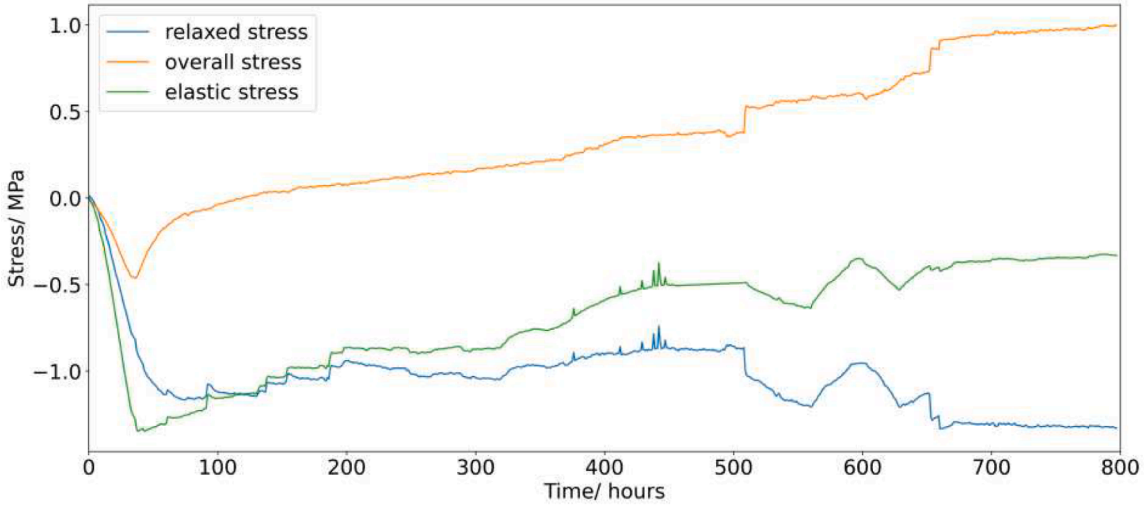

(b) C3-42

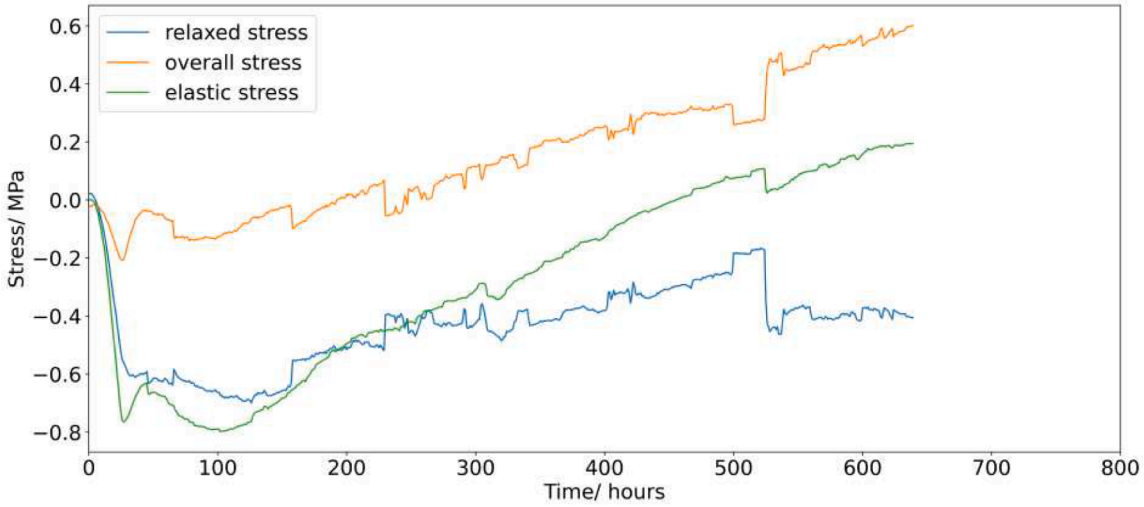

(c) C3-50

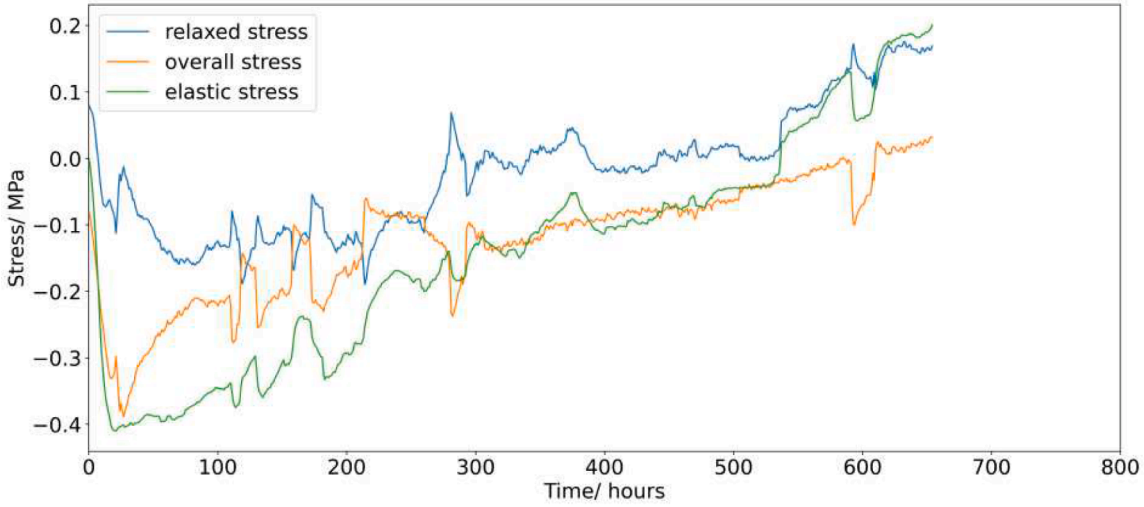

(d) C1-42

Fig. 10. (*continued*).

4. Discussion

Based on the ADTM/ TSTM tests and ESEM/ XRD/ MIP tests conducted in this study, the influence of adding high-volume GGBFS on EAC risk is a complex result of the changes in autogenous deformation and mechanical properties. In the first 2 days after casting, ettringite

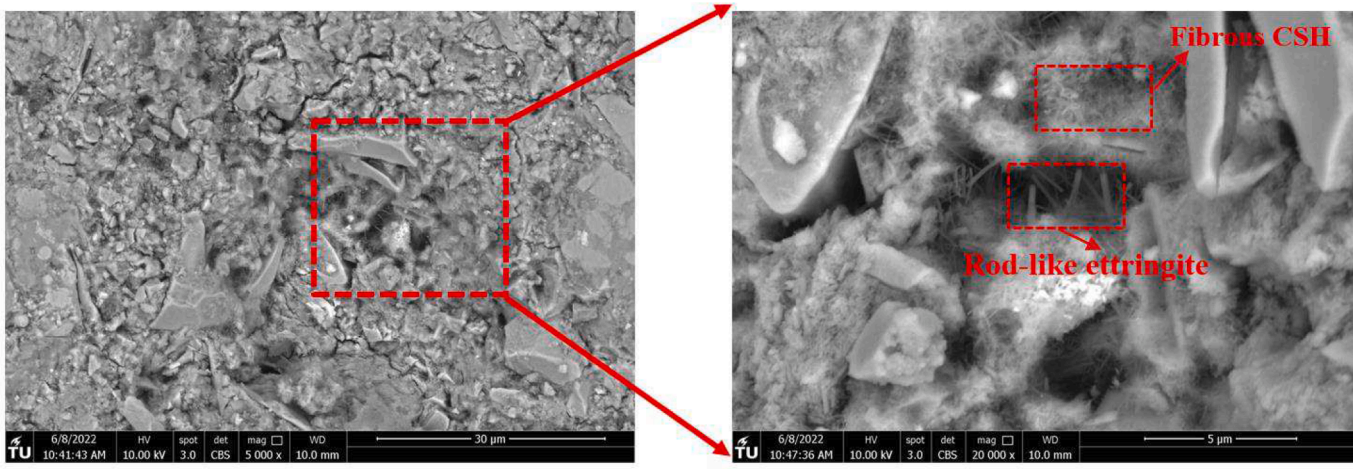

Fig. 11. SEM images of ettringite formation for high volume GGBFS mixes at 1 day (left: porous area; right: zoomed-in view of large pores).

formation induces significant autogenous expansion. After 2 days, GGBFS either acts as filler or promotes the pozzolanic reaction, which contiguously refines the pores and consumes water. As a result, the capillary pressure that can induce autogenous shrinkage is effectively promoted, according to Kelvin's equation. Therefore, in the first 2 days, the influence of GGBFS is favorable for preventing EAC risk, because the high expansion introduces compressive stress and delays the occurrence of tensile stress. However, due to the high early-age creep/ relaxation, most of the compressive stress that should have been accumulated by the autogenous expansion is relaxed. The advantage of the autogenous expansion cannot leverage the increased autogenous shrinkage afterward, and therefore the EAC risk induced by autogenous shrinkage of high-volume GGBFS concrete is higher than that of OPC concrete.

Among the high-volume GGBFS concrete with w/b ratios of 0.35, 0.42, and 0.50, the w/b ratio of 0.42 appears to be the most favorable choice when considering the compressive strength and the EAC risk

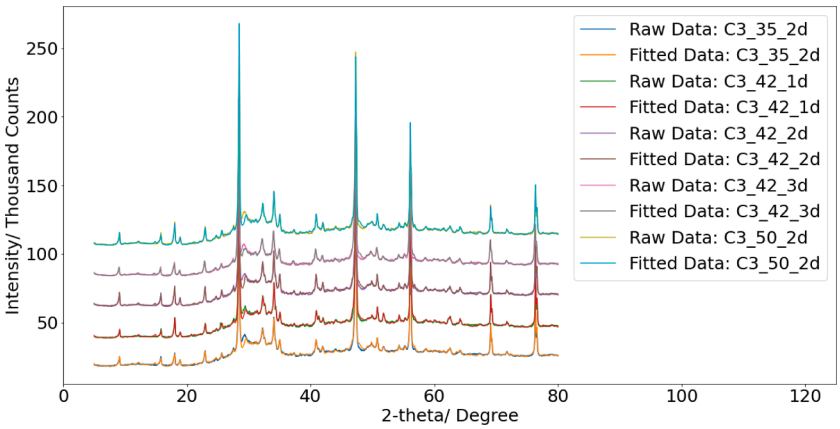

Fig. 12. XRD pattern and Rietveld refinement.

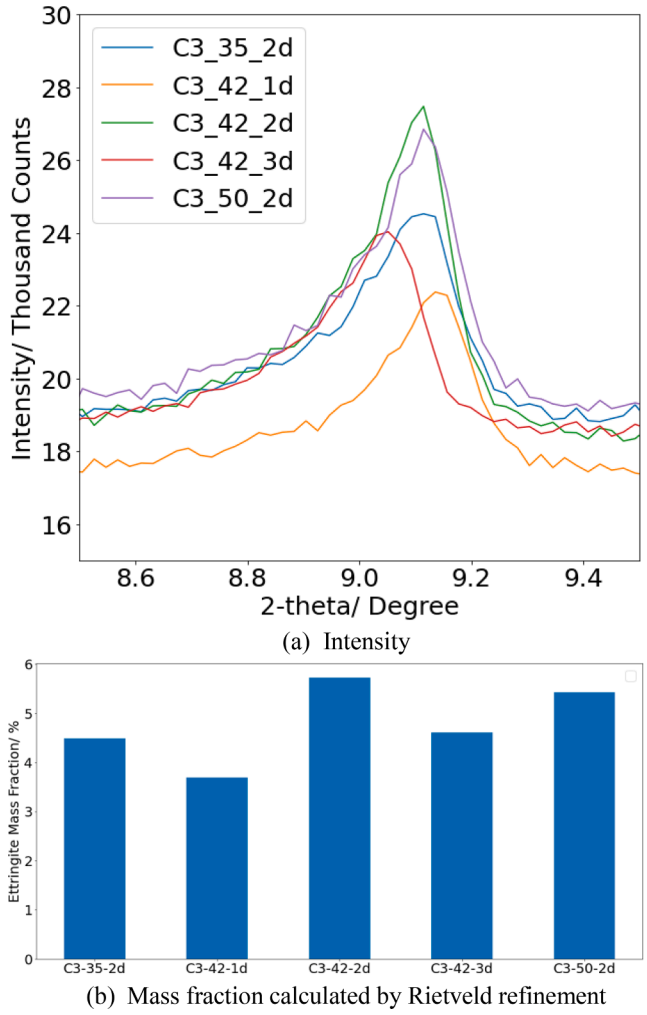

Fig. 13. Ettringite content measured by XRD.

quantified by stress/ strength ratio. Such an advantage is achieved mainly by the compatibility of ettringite formation and pore size evolution. C3-42 generates the highest amount of ettringite which can fill the pores and apply crystalline pressure to induce high autogenous expansion. For the mix C3-35, less ettringite is produced, and therefore only limited autogenous expansion is observed. Afterward, along with the fast decrease of the pore size and the internal relative humidity, the autogenous shrinkage goes fast and results in the rapid increase of tensile stress. For the mix C3-50, although the ettringite amount is comparable with the C3-42, larger pore size limits the effective contact between ettringite and pore walls, and therefore only limited autogenous expansion is observed. However, note that the observations are valid when it comes to autogenous deformation, while when thermal and drying deformation is involved, more factors like the structural sizes need to be considered and thus the final EAC risk for different mixes may change.

The presented study found significant agreement between the macroscale TSTM/ ADTM tests and microscale ESEM/ XRD/ MIP tests, and therefore the major conclusions are valid. However, in the TSTM/ ADTM test results, the fluctuations of measurement with time still indicate a potential error in the macroscale test. This error can be attributed to the temperature instability and the friction between the sample and the supporting plate. Because the dog-bone specimens of TSTM tests are all larger than 1 m, almost all TSTM tests (including this study) are conducted horizontally [58–62]. The self-weight of concrete and the contact between the specimen and the supporting table makes the influence of friction unavoidable, which may further cause jumps in the stress and deformation measurement. Based on the temperature regulating system introduced in section 2.2, the temperature at the middle thermocouple is fixed at 20 degrees. To show how temperature control influences the measurement, the temperature measurement of the C3-42 is given as an example, as shown in Fig. 16. It is found that the temperature in the middle part of the dog-bone specimen was well controlled at 20 degrees, with an error range of 0.05 degree. The temperature at the two ends of the specimen, where water circulation cannot reach, has a temperature close to the room temperature of around 19.5 degrees. To keep the temperature of the middle part specimen at 20 degrees, the water with a temperature of around 20.7 degrees circulates the middle part of the sample. Therefore, the measurement indicates a temperature difference of less than 1 degree exists in both length-wise and depth-wise direction. Moreover, because the room temperature is not stable, it can influence the temperature of the specimen at the two ends directly, and can also influence the feedback control to adjust its water temperature, indicating a change of temperature at the specimen surface also happens. All the factors mentioned above are potentially responsible for measurement jumps in both autogenous deformation and restraint stress.

5. Conclusion

To investigate the EAC risk of high-volume GGBFS concrete, herein ADTM and TSTM tests were conducted to measure the autogenous deformation and induced EAS on high-volume GGBFS concrete with w/b ratios ranging from 0.35 ~ 0.5. Besides, an OPC mix with a medium w/b ratio is also tested as a reference. ESEM/ XRD/ MIP tests were also performed to study the mechanisms of autogenous deformation of

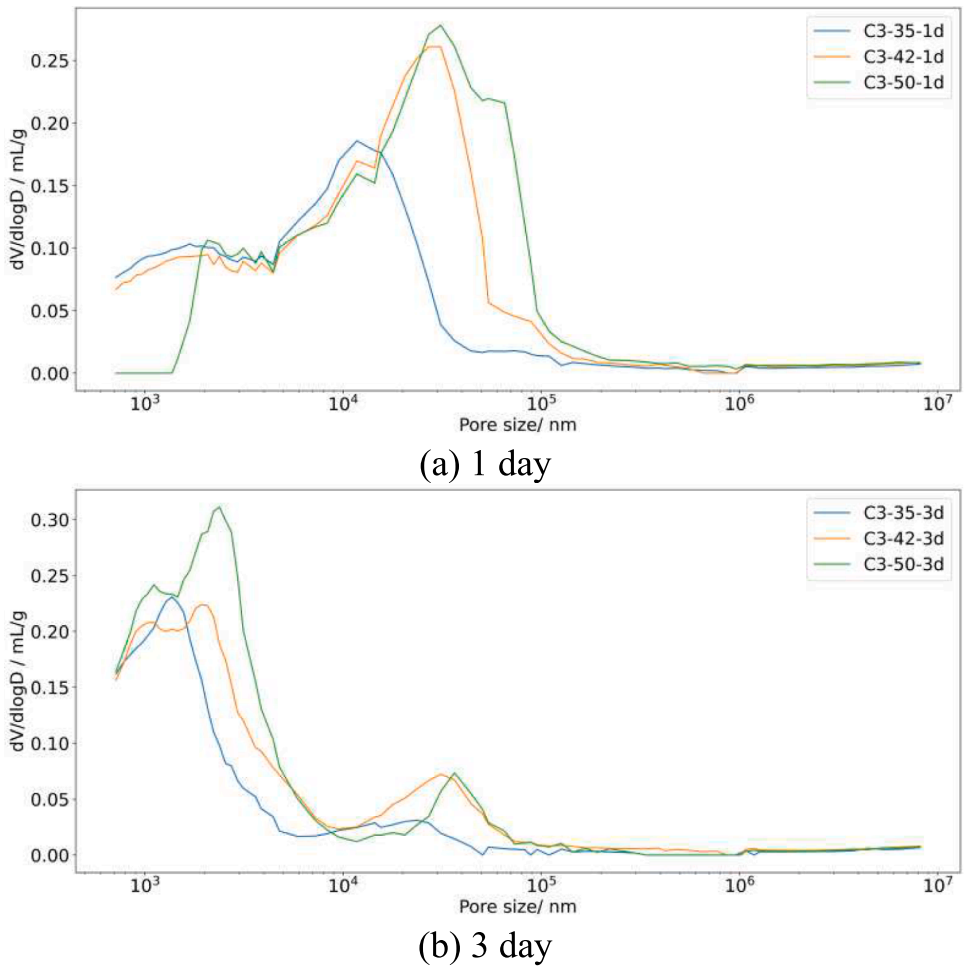

Fig. 14. Pore size distribution derived from MIP results.

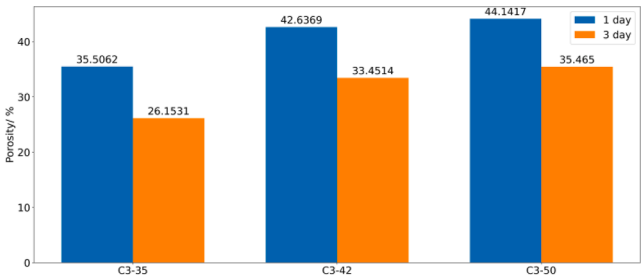

Fig. 15. Porosity of different mixes derived from MIP results.

GGBFS concrete at the microscale. The results of the macro-scale ADTM/ TSTM tests and micro-scale ESEM/ XRD/ MIP tests agree well, which validates the measurement of this study. The following conclusions are available:

i. High-volume GGBFS concrete shows higher autogenous expansion in the first two days and higher autogenous shrinkage afterward than OPC concrete.
ii. The EAC risk induced by autogenous deformation of high-volume GGBFS concrete is higher than OPC concrete, because the compressive stress induced by early-age autogenous expansion is limited by high creep/ relaxation, and the higher autogenous shrinkage of GGBFS concrete plays a more significant role in tensile stress evolution.

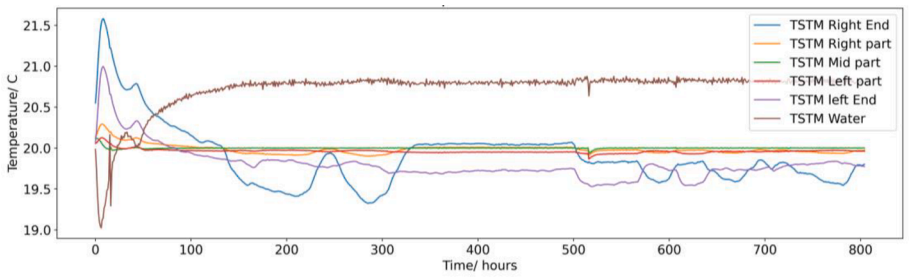

Fig. 16. Temperature measurement of C3-42.

iii. The w/b ratio of 0.42 might be the optimal choice for high-volume GGBFS concrete because it produces the highest amount of ettringite and develops compatible pore size to ensure effective contact between ettringite and pore walls, which further leads to the highest autogenous expansion and therefore high compressive stress as observed in this study.

iv. The w/b ratio of 0.35 appears to be risky for high-volume GGBFS concrete regarding EAC potential. Due to the fast decrease of pore size and porosity, autogenous shrinkage of the high-volume GGBFS concrete with a w/b ratio of 0.35 happens drastically after the expansion peak, which then shows the highest stress/strength ratio.

CRediT authorship contribution statement

Minfei Liang: Conceptualization, Methodology, Formal analysis, Investigation, Data curation, Writing – original draft, Writing – review & editing. **Ze Chang:** Conceptualization, Methodology, Formal analysis, Investigation, Data curation, Writing – original draft, Writing – review & editing. **Yu Zhang:** Investigation, Writing – review & editing. **Hao Cheng:** Investigation, Writing – review & editing. **Shan He:** Investigation, Writing – review & editing. **Erik Schlangen:** Supervision, Funding acquisition, Writing – review & editing. **Branko Šavija:** Supervision, Funding acquisition, Writing – review & editing.

Declaration of Competing Interest

The authors declare that they have no known competing financial interests or personal relationships that could have appeared to influence the work reported in this paper.

Data availability

Data will be made available on request.

Acknowledgment

Minfei Liang, Ze Chang, Yu Zhang, and Hao Cheng would like to acknowledge the funding supported by China Scholarship Council under grant numbers 202007000027, 201806060129, 201808320456, and 202006060024.

References

[1] O. Boukendakdji, E.H. Kadri, S. Kenai, Effects of granulated blast furnace slag and superplasticizer type on the fresh properties and compressive strength of self-compacting concrete, Cem. Concr. Compos. 34 (2012) 583–590, https://doi.org/10.1016/J.CEMCONCOMP.2011.08.013.

[2] S.J. Barnett, M.N. Soutsos, S.G. Millard, J.H. Bungey, Strength development of mortars containing ground granulated blast-furnace slag: Effect of curing temperature and determination of apparent activation energies, Cem. Concr. Res. 36 (2006) 434–440, https://doi.org/10.1016/J.CEMCONRES.2005.11.002.

[3] J.M. Khatib, J.J. Hibbert, Selected engineering properties of concrete incorporating slag and metakaolin, Constr. Build. Mater. 19 (2005) 460–472, https://doi.org/10.1016/J.CONBUILDMAT.2004.07.017.

[4] M.A. Megat Johari, J.J. Brooks, S. Kabir, P. Rivard, Influence of supplementary cementitious materials on engineering properties of high strength concrete, Constr. Build. Mater. 25 (2011) 2639–2648, https://doi.org/10.1016/J.CONBUILDMAT.2010.12.013.

[5] X.Y. Wang, H.S. Lee, K.B. Park, J.J. Kim, J.S. Golden, A multi-phase kinetic model to simulate hydration of slag–cement blends, Cem. Concr. Compos. 32 (2010) 468–477, https://doi.org/10.1016/J.CEMCONCOMP.2010.03.006.

[6] V. Kocaba, E. Gallucci, K.L. Scrivener, Methods for determination of degree of reaction of slag in blended cement pastes, Cem Concr Res. 42 (2012) 511–525, https://doi.org/10.1016/J.CEMCONRES.2011.11.010.

[7] X.Y. Wang, H.S. Lee, Modeling the hydration of concrete incorporating fly ash or slag, Cem. Concr. Res. 40 (2010) 984–996, https://doi.org/10.1016/J.CEMCONRES.2010.03.001.

[8] A. Darquennes, M.I.A. Khokhar, E. Rozière, A. Loukili, F. Grondin, S. Staquet, Early age deformations of concrete with high content of mineral additions, Constr. Build. Mater. 25 (2011) 1836–1847, https://doi.org/10.1016/J.CONBUILDMAT.2010.11.077.

[9] T. Lu, Z. Li, H. Huang, Effect of supplementary materials on the autogenous shrinkage of cement paste, Materials. 13 (2020) 1–15, https://doi.org/10.3390/ma13153367.

[10] T. Lu, Z. Li, K. van Breugel, Modelling of autogenous shrinkage of hardening cement paste, Constr. Build. Mater. 264 (2020) 120708.

[11] P. Lura, O.M. Jensen, J. Weiss, Cracking in cement paste induced by autogenous shrinkage, Materials and Structures/Materiaux et, Constructions 42 (2009) 1089–1099, https://doi.org/10.1617/s11527-008-9445-z.

[12] D. Shen, Y. Jiao, Y. Gao, S. Zhu, G. Jiang, Influence of ground granulated blast furnace slag on cracking potential of high performance concrete at early age, Constr. Build. Mater. 241 (2020) 117839.

[13] M. Bouasker, N.E.H. Khalifa, P. Mounanga, N. ben Kahla, Early-age deformation and autogenous cracking risk of slag–limestone filler-cement blended binders, Constr Build Mater. 55 (2014) 158–167. https://doi.org/10.1016/J.CONBUILDMAT.2014.01.037.

[14] A. Darquennes, S. Staquet, M.P. Delplancke-Ogletree, B. Espion, Effect of autogenous deformation on the cracking risk of slag cement concretes, Cem. Concr. Compos. 33 (2011) 368–379, https://doi.org/10.1016/j.cemconcomp.2010.12.003.

[15] D. Shen, K. Liu, C. Wen, Y. Shen, G. Jiang, Early-age cracking resistance of ground granulated blast furnace slag concrete, Constr Build Mater. 222 (2019) 278–287, https://doi.org/10.1016/j.conbuildmat.2019.06.028.

[16] Y. Wei, W. Hansen, Early-age strain–stress relationship and cracking behavior of slag cement mixtures subject to constant uniaxial restraint, Constr. Build. Mater. 49 (2013) 635–642, https://doi.org/10.1016/J.CONBUILDMAT.2013.08.061.

[17] A. Markandeya, N. Shanahan, D.M. Gunatilake, K.A. Riding, A. Zayed, Influence of slag composition on cracking potential of slag-portland cement concrete, Constr. Build. Mater. 164 (2018) 820–829, https://doi.org/10.1016/j.conbuildmat.2017.12.216.

[18] L. Wu, N. Farzadnia, C. Shi, Z. Zhang, H. Wang, Autogenous shrinkage of high performance concrete: A review, Constr. Build. Mater. 149 (2017) 62–75, https://doi.org/10.1016/j.conbuildmat.2017.05.064.

[19] K.M. Lee, H.K. Lee, S.H. Lee, G.Y. Kim, Autogenous shrinkage of concrete containing granulated blast-furnace slag, Cem. Concr. Res. 36 (2006) 1279–1285, https://doi.org/10.1016/J.CEMCONRES.2006.01.005.

[20] E. Ghafari, S.A. Ghahari, H. Costa, E. Júlio, A. Portugal, L. Durães, Effect of supplementary cementitious materials on autogenous shrinkage of ultra-high performance concrete, Constr. Build. Mater. 127 (2016) 43–48, https://doi.org/10.1016/J.CONBUILDMAT.2016.09.123.

[21] B. Hilloulin, V.Q. Tran, Using machine learning techniques for predicting autogenous shrinkage of concrete incorporating superabsorbent polymers and supplementary cementitious materials, Journal of Building Engineering. 49 (2022), 104086, https://doi.org/10.1016/j.jobe.2022.104086.

[22] A. Darquennes, B. Espion, S. Staquet, How to assess the hydration of slag cement concretes? Constr. Build. Mater. 40 (2013) 1012–1020, https://doi.org/10.1016/j.conbuildmat.2012.09.087.

[23] S.J. Lokhorst, Deformational Behaviour of Concrete Influenced by Hydration Related Changes of the Microstructure, Delft University of Technology, 2001.

[24] P. Lura, J. Couch, O.M. Jensen, J. Weiss, Early-age acoustic emission measurements in hydrating cement paste: Evidence for cavitation during solidification due to self-desiccation, Cem. Concr. Res. 39 (2009) 861–867, https://doi.org/10.1016/j.cemconres.2009.06.015.

[25] T. Lu, Z. Li, H. Huang, Restraining effect of aggregates on autogenous shrinkage in cement mortar and concrete, Constr. Build. Mater. 289 (2021), 123166, https://doi.org/10.1016/J.CONBUILDMAT.2021.123166.

[26] O. Mejlhede Jensen, P. Freiesleben Hansen, A dilatometer for measuring autogenous deformation in hardening portland cement paste, Mater. Struct. 28 (1995) 406–409, https://doi.org/10.1007/BF02473076.

[27] Y. Zhang, S. Zhang, Y. Chen, O. Çopuroğlu, The effect of slag chemistry on the reactivity of synthetic and commercial slags, Constr. Build. Mater. 335 (2022), 127493, https://doi.org/10.1016/J.CONBUILDMAT.2022.127493.

[28] R.J. Flatt, G.W. Scherer, Thermodynamics of crystallization stresses in DEF, Cem. Concr. Res. 38 (2008) 325–336, https://doi.org/10.1016/J.CEMCONRES.2007.10.002.

[29] P. Lura, O.M. Jensen, K. van Breugel, Autogenous shrinkage in high-performance cement paste: An evaluation of basic mechanisms, Cem. Concr. Res. 33 (2003) 223–232, https://doi.org/10.1016/S0008-8846(02)00890-6.

[30] Modelling of autogenous shrinkage of cement paste, (n.d.).

[31] L. Barcelo, M. Moranville, B. Clavaud, Autogenous shrinkage of concrete: A balance between autogenous swelling and self-desiccation, Cem. Concr. Res. 35 (2005) 177–183, https://doi.org/10.1016/j.cemconres.2004.05.050.

[32] K. Scrivener, R. Snellings, B. Lothenbach, A practical guide to microstructural analysis of cementitious materials, n.d.

[33] S. Diamond, Mercury porosimetry: An inappropriate method for the measurement of pore size distributions in cement-based materials, Cem. Concr. Res. 30 (2000) 1517–1525, https://doi.org/10.1016/S0008-8846(00)00370-7.

[34] C. Gallé, Effect of drying on cement-based materials pore structure as identified by mercury intrusion porosimetry, Cem. Concr. Res. 31 (2001) 1467–1477, https://doi.org/10.1016/S0008-8846(01)00594-4.

[35] R. Kumar, B. Bhattacharjee, Study on some factors affecting the results in the use of MIP method in concrete research, Cem. Concr. Res. 33 (2003) 417–424, https://doi.org/10.1016/S0008-8846(02)00974-2.

[36] J. Zhao, D. Wang, P. Yan, Design and experimental study of a ternary blended cement containing high volume steel slag and blast-furnace slag based on Fuller distribution model, Constr. Build. Mater. 140 (2017) 248–256, https://doi.org/10.1016/J.CONBUILDMAT.2017.02.119.

[37] K. Meinhard, R. Lackner, Multi-phase hydration model for prediction of hydration-heat release of blended cements, Cem. Concr. Res. 38 (2008) 794–802, https://doi.org/10.1016/J.CEMCONRES.2008.01.008.
[38] E.-I. Tazawa, S. Miyazawa, Influence of cement and admixture on autogenous shrinkage of cement paste, Cem. Concr. Res. 25 (2) (1995) 281–287.
[39] C. Jiang, Y. Yang, Y. Wang, Y. Zhou, C. Ma, Autogenous shrinkage of high performance concrete containing mineral admixtures under different curing temperatures, Constr. Build. Mater. 61 (2014) 260–269, https://doi.org/10.1016/J.CONBUILDMAT.2014.03.023.
[40] M.H. Zhang, C.T. Tam, M.P. Leow, Effect of water-to-cementitious materials ratio and silica fume on the autogenous shrinkage of concrete, Cem. Concr. Res. 33 (2003) 1687–1694, https://doi.org/10.1016/S0008-8846(03)00149-2.
[41] D. Shen, J. Jiang, J. Shen, P. Yao, G. Jiang, Influence of curing temperature on autogenous shrinkage and cracking resistance of high-performance concrete at an early age, Constr. Build. Mater. 103 (2016) 67–76, https://doi.org/10.1016/J.CONBUILDMAT.2015.11.039.
[42] M.A. Rashid, M.A. Mansur, P. Paramasivam, Correlations between Mechanical Properties of High-Strength Concrete, J. Mater. Civ. Eng. 14 (2002) 230–238, https://doi.org/10.1061/(ASCE)0899-1561(2002)14:3(230).
[43] Y. Choi, R.L. Yuan, Experimental relationship between splitting tensile strength and compressive strength of GFRC and PFRC, Cem. Concr. Res. 35 (2005) 1587–1591, https://doi.org/10.1016/J.CEMCONRES.2004.09.010.
[44] M.F.M. Zain, H.B. Mahmud, A. Ilham, M. Faizal, Prediction of splitting tensile strength of high-performance concrete, Cem. Concr. Res. 32 (2002) 1251–1258, https://doi.org/10.1016/S0008-8846(02)00768-8.
[45] fib, fib Model Code for Concrete Structures 2010, Wiley-VCH Verlag GmbH & Co. KGaA, Weinheim, Germany, 2013. https://doi.org/10.1002/9783433604090.
[46] P. Virtanen, R. Gommers, T.E. Oliphant, M. Haberland, T. Reddy, D. Cournapeau, E. Burovski, P. Peterson, W. Weckesser, J. Bright, S.J. van der Walt, M. Brett, J. Wilson, K.J. Millman, N. Mayorov, A.R.J. Nelson, E. Jones, R. Kern, E. Larson, C. J. Carey, İ. Polat, Y.u. Feng, E.W. Moore, J. VanderPlas, D. Laxalde, J. Perktold, R. Cimrman, I. Henriksen, E.A. Quintero, C.R. Harris, A.M. Archibald, A.H. Ribeiro, F. Pedregosa, P. van Mulbregt, A. Vijaykumar, A.P. Bardelli, A. Rothberg, A. Hilboll, A. Kloeckner, A. Scopatz, A. Lee, A. Rokem, C.N. Woods, C. Fulton, C. Masson, C. Häggström, C. Fitzgerald, D.A. Nicholson, D.R. Hagen, D. V. Pasechnik, E. Olivetti, E. Martin, E. Wieser, F. Silva, F. Lenders, F. Wilhelm, G. Young, G.A. Price, G.-L. Ingold, G.E. Allen, G.R. Lee, H. Audren, I. Probst, J. P. Dietrich, J. Silterra, J.T. Webber, J. Slavič, J. Nothman, J. Buchner, J. Kulick, J. L. Schönberger, J.V. de Miranda Cardoso, J. Reimer, J. Harrington, J.L. C. Rodríguez, J. Nunez-Iglesias, J. Kuczynski, K. Tritz, M. Thoma, M. Newville, M. Kümmerer, M. Bolingbroke, M. Tartre, M. Pak, N.J. Smith, N. Nowaczyk, N. Shebanov, O. Pavlyk, P.A. Brodtkorb, P. Lee, R.T. McGibbon, R. Feldbauer, S. Lewis, S. Tygier, S. Sievert, S. Vigna, S. Peterson, S. More, T. Pudlik, T. Oshima, T.J. Pingel, T.P. Robitaille, T. Spura, T.R. Jones, T. Cera, T. Leslie, T. Zito, T. Krauss, U. Upadhyay, Y.O. Halchenko, Y. Vázquez-Baeza, SciPy 1.0: fundamental algorithms for scientific computing in Python, Nat. Methods 17 (3) (2020) 261–272.
[47] M. Liang, Z. Chang, Z. Wan, Y. Gan, E. Schlangen, B. Šavija, Interpretable Ensemble-Machine-Learning models for predicting creep behavior of concrete, Cem. Concr. Compos. 125 (2022), 104295, https://doi.org/10.1016/J.CEMCONCOMP.2021.104295.
[48] M. Liang, Y. Gan, Z. Chang, Z. Wan, E. Schlangen, B. Šavija, Microstructure-informed deep convolutional neural network for predicting short-term creep modulus of cement paste, Cem. Concr. Res. 152 (2022), 106681, https://doi.org/10.1016/J.CEMCONRES.2021.106681.
[49] M. Azenha, F. Kanavaris, D. Schlicke, A. Jędrzejewska, F. Benboudjema, T. Honorio, V. Šmilauer, C. Serra, J. Forth, K. Riding, B. Khadka, C. Sousa, M. Briffaut, L. Lacarrière, E. Koenders, T. Kanstad, A. Klausen, J.M. Torrenti, E.M. R. Fairbairn, Recommendations of RILEM TC 287-CCS: thermo-chemo-mechanical modelling of massive concrete structures towards cracking risk assessment, Materials and Structures/Materiaux et Constructions. 54 (2021) 135, https://doi.org/10.1617/s11527-021-01732-8.
[50] M. Liang, Z. Li, S. He, Z. Chang, Y. Gan, E. Schlangen, B. Šavija, Stress evolution in restrained GGBFS concrete due to autogenous deformation: bayesian optimization of aging creep, Constr. Build. Mater. 324 (2022), 126690, https://doi.org/10.1016/J.CONBUILDMAT.2022.126690.
[51] B. Delsaute, C. Boulay, S. Staquet, Creep testing of concrete since setting time by means of permanent and repeated minute-long loadings, Cem. Concr. Compos. 73 (2016) 75–88, https://doi.org/10.1016/J.CEMCONCOMP.2016.07.005.
[52] B. Delsaute, J.M. Torrenti, S. Staquet, Modeling basic creep of concrete since setting time, Cem. Concr. Compos. 83 (2017) 239–250, https://doi.org/10.1016/j.cemconcomp.2017.07.023.
[53] H. Beushausen, T. Dittmer, The influence of aggregate type on the strength and elastic modulus of high strength concrete, Constr Build Mater. 74 (2015) 132–139, https://doi.org/10.1016/J.CONBUILDMAT.2014.08.055.
[54] M. Gesoğlu, E. Güneyisi, T. Özturan, Effects of end conditions on compressive strength and static elastic modulus of very high strength concrete, Cem. Concr. Res. 32 (2002) 1545–1550, https://doi.org/10.1016/S0008-8846(02)00826-8.
[55] F.P. Zhou, F.D. Lydon, B.I.G. Barr, Effect of coarse aggregate on elastic modulus and compressive strength of high performance concrete, Cem. Concr. Res. 25 (1995) 177–186, https://doi.org/10.1016/0008-8846(94)00125-I.
[56] H.M. Rietveld, A Profile Refinement Method for Nuclear and Magnetic Structures, J. Appl. Cryst. 2 (1969) 65–71.
[57] N. Doebelin, R. Kleeberg, Profex: A graphical user interface for the Rietveld refinement program BGMN, J. Appl. Cryst. 48 (5) (2015) 1573–1580.
[58] A.E. Klausen, Early age crack assessment of concrete structures, experimental determination of decisive parameters, Ph.D. thesis, NTNU (2016).
[59] Ø. Bjøntegaard, Termal dilation and autogenous deformation as driving forces to self-induced stresses in high performance concrete, Norwegian University of Science and Technology (NTNU), 1999. Ph.D. thesis.
[60] R. Springenschmid, R. Breitenbücher, M. Mangold, Development of the cracking frame and the temperature-stress testing machine, in: Proceedings of the International RILEM Symposium, Munich, Germany, 1994: pp. 137–144.
[61] G. Ou, Z. Lin, T. Kishi, The practical application of a self-developed temperature stress testing machine in development of expansive concrete blended with calcium sulfoaluminate additives, Cem. Concr. Res. 164 (2023), 107045, https://doi.org/10.1016/j.cemconres.2022.107045.
[62] S. Staquet, B. Delsaute, A. Darquennes, B. Espion, Design of a revisited TSTM system for testing concrete since setting time under free and restraint conditions, in: CONCRACK 3 – RILEM-JCI International Workshop on Crack Control of Mass Concrete and Related Issues Concerning Early-Age of Concrete Structures, Paris, France, 2012.